

Spatiotemporal Flat Field of the Gated Optical Imager Used on the 3ω Beamlets Diagnostic

J. Katz, N. Whiting, and S. T. Ivancic

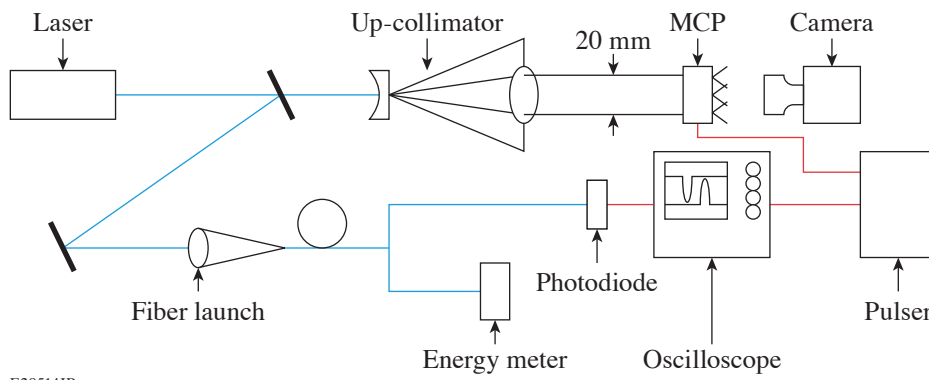
Laboratory for Laser Energetics, University of Rochester

Introduction

Gated optical imagers (GOI's) use microchannel-plate (MCP)-type intensifier tubes to electronically control the exposure duration of a 2-D image. Short exposure durations can be used to reduce motion blur in a dynamic scene or reject late-time sources of background noise such as ghost reflections or persistent thermal emission. The current state-of-the-art high-speed GOI's that use 18-mm-diam image tubes can achieve gate times of the order of 100 ps (Refs. 1 and 2). In the gated-off state, the entrance face of the MCP is negatively biased relative to the photocathode, preventing the flow of electrons to the MCP. The tube is gated on by applying a positive voltage pulse to a photocathode that temporarily overcomes a preimposed bias. Photoelectrons can then pass through the MCP amplification stage and are imaged on a phosphor screen. The MCP tube geometry and electrical capacitance of the photocathode influence the speed at which a transient voltage can be applied to the tube surface. In the fastest regimes the gating process is both spatially and temporally dynamic. Different regions of the image see different on/off times and exposure durations as the gate pulse propagates across the photocathode. Quantitative knowledge of the overall detector sensitivity as a function of position and time is required to accurately compare data recorded at different image positions. This type of calibration is critical to the 3ω beamlets diagnostic on OMEGA, which simultaneously records a four-frame image on a single exposure.³ The beamlet energy, polarization state, and temporal evolution are determined by comparing the individual beamlet signals in each subimage.

Calibration Apparatus

A short-pulse laser was used to map out the optical gate profile over a series of image acquisitions by triggering the GOI at different times with respect to the incoming pulse (Fig. 1). A frequency-doubled Ti:sapphire ($\lambda = 395$ -nm) laser with 1-ps pulse duration was up-collimated to ~20-mm diameter and free-space propagated to the GOI photocathode. The up-collimator produced a relatively flattop beam profile by selecting only the central 1/10th of the original Gaussian laser near field. A sample of the laser pulse was split and fiber coupled for use as an energy and timing reference. Once fiber coupled, the pulse was split again with one leg sent to a time-integrated energy meter and the second leg sent to a high-speed (90-ps) photodiode. The photodiode output and an electrical monitor pulse produced from the GOI pulser were recorded on separate channels of an 8-GHz oscilloscope



E28514JR

Figure 1

A laser with 1-ps pulse duration is used to characterize the GOI gate as a function of time and image position. The arrival time of the laser pulse relative to the GOI trigger is varied over a series of image acquisitions to map out the gate profile. An oscilloscope measures the laser timing relative to a monitor of the GOI gating pulse. The energy of each incident pulse is quantified using an energy meter.

sampling at 40 Gs/s. The relative trigger time for each image frame was measured by comparing the reference pickoff timing to the monitor pulse and was determined with 5-ps accuracy. The pulse energy was also measured by integrating the photodiode oscilloscope trace. Agreement between the two pulse energy measurements was 2.5% rms, allowing fluctuations in laser pulse energy to be corrected for in each image frame.

Generation of a Flat-Field Calibration

To establish the baseline spatial uniformity of the illumination beam, a series of images were collected with the GOI in slow gate exposure mode. The slow gate setting provides millisecond exposure durations using separate gating circuitry. The flat-field images are used to quantify intensity nonuniformities introduced by the laser near field, diffraction from the up-collimator, and dust particles on the transport optics. The scan of the fast gate included \sim 85 shots. A system jitter of \pm 50 ps prevents the scan from being generated with equal spacing time steps but timing information can be recovered to \pm 5 ps by fitting the monitor and diode traces in post-processing. By sorting the acquisitions by trigger time, a gain history with approximately 5-ps sample intervals is generated. As shown in Fig. 2(a), the 3 ω beamlets' GOI has an exposure duration of approximately 250 ps. A sensitivity figure of merit $G(x,y)$ is calculated by integrating the gate history as a function of time on a pixel-by-pixel basis, given by Eq. (1).

$$G(x,y) = \frac{1}{\text{FF}(x,y)} \sum_i^n \frac{I_{i+1}(x,y) + I_i(x,y)}{2E_i} (t_{i+1} - t_i), \quad (1)$$

where $I(x,y)$ is the signal intensity of a given image pixel on the i th image in the set, t_i is the relative time that the image was acquired, E_i is the corresponding pulse energy, and FF is the normalized image from the slow-gate flat field. Equation (1) generates a composite image that contains the time-integrated gain sensitivity as a function of image position [Fig. 2(b)].

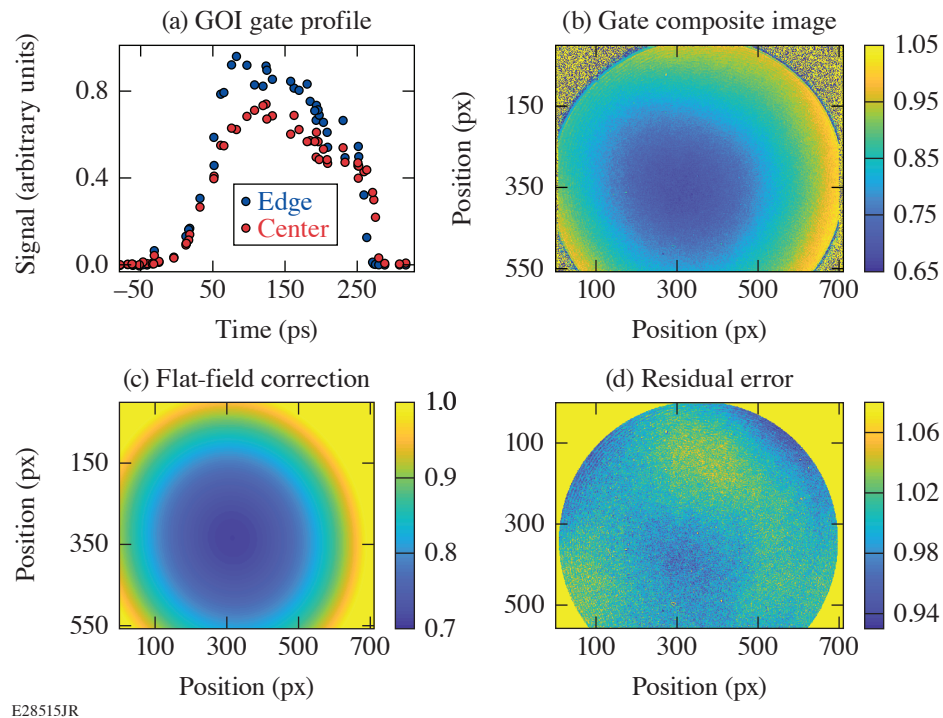


Figure 2

(a) The gain as a function of time is shown at two different pixel locations on the GOI image. (b) A composite image is generated by integrating the gain history at each point in the image. (c) The flat-field calibration function is generated by fitting the composite image fit with a 2-D second-order polynomial. (d) Dividing the composite image by the flat-field function corrects the spatial variations in gain to 2.2% rms.

Figure 2(b) shows the measured sensitivity as a function of image position. The edges of the MCP tube are more sensitive than the center. The magnitude of sensitivity variation is a function of bias voltage. In general, faster gate times can be achieved for a given electrical gate pulse by increasing the MCP to photocathode bias. In this case, electrons flow only during the peak portion of the gate pulse. However, this also results in a lower electron extraction field, making the gating process more sensitive to variations in extraction field uniformity. Excessive bias produces fast gate profiles but can result in a complete lack of sensitivity in the image center. Ultimately the bias setting is a compromise between spatial sensitivity uniformity and gate speed. Recording the spatiotemporal flat field at different settings allows the bias voltage to be optimized. In the case of the standard beamlets configuration, the 250-ps gate duration is accompanied by a 40% peak-to-valley (p–v) variation in sensitivity from the image center to the edge.

A smooth and continuous calibration function was generated from the composite gate image by fitting it to a 2-D second-order polynomial [Fig. 2(c)]. The fitting process averages out pixel-to-pixel statistical noise and smooths residual features from diffraction and dust that persisted after flat fielding. Figure 2(d) shows the residual sensitivity variation of the original composite image after the flat-field correction. Dividing the composite image by the correction function results in a 2.2% rms variation in measured signal intensity with a p–v of ~6%.

Conclusions

A short-pulse laser and precision trigger monitor system were used to generate a spatiotemporal flat field for a high-speed GOI used in the 3ω beamlets. Measuring the detector sensitivity as a function of time and image position makes it possible to optimize the GOI operating voltages. A method for averaging calibration data into a single scalar correction function is described. Implementation of the correction function reduces spatial gain variations from ~40% p–v and 9.3% rms to 6% p–v and 2.2% rms.

This material is based upon work supported by the Department of Energy National Nuclear Security Administration under Award Number DE-NA0003856, the University of Rochester, and the New York State Energy Research and Development Authority.

1. P. E. Young *et al.*, Rev. Sci. Instrum. **59**, 1457 (1988).
2. B. Little, Rev. Sci. Instrum. **89**, 10E117 (2018).
3. D. H. Edgell *et al.*, Rev. Sci. Instrum. **89**, 10E101 (2018).